Thyrocyte-specific deletion of insulin and IGF-1 receptors induces papillary thyroid carcinoma-like lesions through EGFR pathway activation

Sangmi Ock[1], Jihyun Ahn[1], Seok Hong Lee[1], Hyun Min Kim[1], Hyun Kang[2], Young-Kook Kim[3], Hyun Kook[4], Woo Jin Park[5], Shin Kim[6], Shioko Kimura[7], Chan Kwon Jung[8], Minho Shong[9], Martin Holzenberger[10], E. Dale Abel[11], Tae Jin Lee[12], Bo Youn Cho[1], Ho-Shik Kim[13] and Jaetaek Kim [1]

[1]Division of Endocrinology and Metabolism, Department of Internal Medicine, College of Medicine, Chung-Ang University, Seoul, Korea
[2]Department of Anesthesiology, College of Medicine, Chung-Ang University, Seoul, Korea
[3]Department of Biochemistry, Chonnam National University Medical School, Gwangju, Korea
[4]Department of Pharmacology and Medical Research Center for Gene Regulation, Chonnam National University Medical School, Gwangju, Korea
[5]Department of Life Science, Gwangju Institute of Science and Technology, Gwangju, Korea
[6]Department of Immunology, Keimyung University School of Medicine, Daegu, Korea
[7]Laboratory of Metabolism, National Cancer Institute, National Institutes of Health, Bethesda, MD, USA
[8]Department of Hospital Pathology, College of Medicine, The Catholic University of Korea, Seoul, Korea
[9]Research Center for Endocrine and Metabolic Diseases, Department of Internal Medicine, Chungnam National University, Daejeon, Korea
[10]INSERM and Sorbonne University, Saint-Antoine Research Center, Paris, France
[11]Fraternal Order of Eagles Diabetes Research Center and Division of Endocrinology and Metabolism, University of Iowa Carver College of Medicine, Iowa City, IA, USA
[12]Department of Pathology, College of Medicine, Chung-Ang University, Seoul, Korea
[13]Department of Biochemistry, College of Medicine, The Catholic University of Korea, Seoul, Korea

Insulin and insulin-like growth factor (IGF)-1 signaling in the thyroid are thought to be permissive for the coordinated regulation by thyroid-stimulating hormone (TSH) of thyrocyte proliferation and hormone production. However, the integrated role of insulin receptor (IR) and IGF-1 receptor (IGF-1R) in thyroid development and function has not been explored. Here, we generated thyrocyte-specific IR and IGF-1R double knockout (DTIRKO) mice to precisely evaluate the coordinated functions of these receptors in the thyroid of neonates and adults. Neonatal DTIRKO mice displayed smaller thyroids, paralleling defective folliculogenesis associated with repression of the thyroid-specific transcription factor Foxe1. By contrast, at postnatal day 14, absence of IR and IGF-1R paradoxically induced thyrocyte proliferation, which was mediated by mTOR-dependent signaling pathways. Furthermore, we found elevated production of TSH during the development of follicular hyperplasia at 8 weeks of age. By 50 weeks, all DTIRKO mice developed papillary thyroid carcinoma (PTC)-like lesions that correlated with induction of the ErbB pathway. Taken together, these data define a critical role for IR and IGF-1R in neonatal thyroid folliculogenesis. They also reveal an important reciprocal relationship between IR/IGF-1R and TSH/ErbB signaling in the pathogenesis of thyroid follicular hyperplasia and, possibly, of papillary carcinoma.

What's new?

Loss of insulin-like growth factor-1 receptor (IGF-1R) in the thyroid results in chronic signaling by thyroid stimulating hormone. Little is known, however, about the consequences of IGF-1R deletion or the loss insulin receptor (IR). Here, using a thyrocyte-specific IR and IGF-1R double knockout mouse model, the authors show that IR/IGF-1R signaling in the thyroid is necessary for normal folliculogenesis. While thyroid size was smaller in neonatal knockout animals, IR/IGF-1R loss paradoxically induced thyrocyte proliferation at postnatal day 14, a process mediated by mTOR-dependent signaling. Papillary thyroid carcinoma-like lesions were later detected in aged double knockout mice.

Introduction

The thyroid gland consists of functional units, follicles that are spheroidal structures composed of thyroid hormone-storing colloid surrounded by a monolayer of polarized cells, called follicular cells or thyrocytes.[1] Thyroid-stimulating hormone (TSH) is a major regulator of thyroid structure and function in adults. TSH regulates biosynthesis, storage and secretion of two thyroid hormones, triiodothyronine (T_3) and thyroxine (T_4) and stimulates thyrocyte proliferation, aggregation of thyrocytes into follicles and maintenance of the follicular architecture.[2] Although mice with constitutive TSH receptor (TSHR) knockout display hypothyroidism and thyroid hypoplasia as adults, thyroid folliculogenesis and gland size in the prenatal period are normal.[3,4] Thus, TSH does not seem to participate in controlling the differentiation and morphogenesis of the developing thyroid. These findings suggest that signaling from other growth factors might regulate thyroid growth during the prenatal period.

Thyroid follicle development is regulated by thyroid transcription factors (TTFs), such as forkhead box E1 (Foxe1), NK2 homeobox 1 (Nkx2–1), paired homeobox 8 (Pax8) and hematopoietically expressed homeobox protein Hhex (Hhex) at embryonic day 8.5 (E8.5) in mice.[5] The coordinated expression of TTFs is essential for thyroid development and the induction of thyroid-specific genes including thyroglobulin (*Tg*), thyroid peroxidase (*Tpo*), the sodium iodide symporter (*Nis*), dual oxidase 2 (*Duox*) and *Tshr*. However, the upstream regulators of TTFs are not well understood. Insulin and insulin-like growth factor-1 (IGF-1) play pleiotropic roles in energy metabolism, development and growth.[6] It has been widely accepted that IGF-1 interacts with TSH in regulating thyroid growth.[7,8] When added to cultured thyrocytes, insulin and IGF-1 modulate the levels of Foxe1, a key transcription factor involved in thyroid morphogenesis.[9] We previously reported that thyrocyte-specific insulin receptor (IR) deficient (TIRKO) or IGF-1R deficient (TIGF1RKO) mice retain normal postnatal thyroid development, suggesting functional redundancy of IR and IGF-1R signaling in postnatal folliculogenesis.[10,11] This prompted us to investigate the effects of combined deletion of the IR and IGF-1R on the thyroid development.

IGF-1R deletion in the thyroid unexpectedly induces a proliferative phenotype under chronic TSH stimulation.[12] However, the long-term consequences of deletion of both IR and IGF-1R and its impact on the induction of other growth factors that could be modulated by these receptors *per se* or by persistent TSH signaling remain incompletely understood. Thus, to clarify whether IR and IGF-1R cooperatively regulate postnatal thyroid development, we generated thyrocyte-specific IR/IGF-1R double knockout (DTIRKO) mice. In our study, we demonstrate that both IR and IGF-1R are essential for the maintenance of the normal follicular architecture of the neonatal thyroid. Surprisingly, simultaneous deletion of these receptors leads to paradoxical follicular hyperplasia and papillary thyroid carcinoma (PTC)-like lesions via mechanisms that may include augmented TSH signaling and interdependent ErbB pathway hyperactivation.

Materials and Methods

Generation of DTIRKO mice

Mice homozygous for floxed IR and IGF-1R alleles in which loxP sites flank exon 3 of the respective gene ($IR^{lox/lox}$; IGF-$1R^{lox/lox}$)[10,11] were crossed with mice that express *Cre* recombinase specifically in thyrocytes under control of the thyroglobulin (Tg) gene promoter.[13] Pups were born in the expected Mendelian ratios and litter size was normal, indicating that the floxed alleles had no effect on embryonic and perinatal viability. To confirm thyrocyte-specific Cre-mediated recombination of exon 3, triplex PCR was performed with primers 5′-CCATGGGTGTTAAATGTAATGGC-3′, 5′-ATGAATGCTGGTGAGGGTTGTCTT-3′ and 5′-ATCTTG-GAGTGGTGGGTCTGTTTC-3′. Animals were fed standard chow and autoclaved water *ad libitum*, housed in temperature-controlled, pathogen-free facilities with a 12 h light/dark cycle. All animals were maintained on a C57BL/6 background and male mice were used in our study. All animal experiments were conducted in accordance with guidelines approved by the institutional animal care and use committee of the Chung-Ang University.

Tissue preparation and immunohistochemistry

Analyses were performed as described.[11] Slides with 4 μm tissue sections de-paraffinized at 55–60 °C for 1 h were incubated twice in 100% xylene 3 times for 5 min each and hydrated through an ethanol series 100, 95, 85 and 75% for 5 min each. After washing in PBS, slides were stained with H&E solution, and then dehydrated in ethanol (75, 85, 95 and 100%) for 5 min at each concentration, followed by 100% xylene 3 times for 5 min each. Slides were mounted using coverslips and mounting medium. The sections were examined using a Leica DM500 microscope and the following

parameters were measured using NIH ImageJ software. Briefly, from each section, 30 randomly selected thyroid follicles were analyzed for cross sectional area, follicle area, colloid area, thyrocyte size and number of nuclei.

For immunohistochemical analysis, thyroid tissues fixed in 4% paraformaldehyde were embedded in paraffin or OCT medium and frozen. Paraffin sections (4 μm) were deparaffinized with xylene and rehydrated in graded alcohol series, then washed in. After antigen retrieval was performed in citrate butter (pH 6.0) or Tris-EDTA buffer (pH 9.0) at 121 °C for 3 min, endogenous peroxidase was quenched by 3% H_2O_2 in TDW for 10 min. Frozen sections (6 μm) were air-dried for 3 min at room temperature, then washed in TDW. After endogenous peroxidase was quenched by 3% H_2O_2 in methanol for 15 min, antigen retrieval was performed in citrate butter (pH 6.0) at 100 °C for 20 min. Non-specific staining of paraffin or frozen sections was blocked with 10% normal serum, and then sections were incubated with primary antibodies for 30 min at 37 °C. The primary antibodies used in our study were commercially obtained. See Supporting Information Table S1 for antibodies used. The sections were then incubated with peroxidase-conjugated streptavidin for 45 min, followed by color development with diaminobenzidine. For quantification of the Nkx2–1, Foxe1, or Pax8 positive cells, at least 300 randomly selected thyroid nuclei were analyzed. Relative numbers of Nkx2–1 or Pax8 positive cells were calculated as the number of positive nuclei divided by the number of total nuclei. While Foxe1 was reported to be expressed in both the nucleus and cytoplasm,[14] relative numbers of Foxe1-positive cells were calculated as the number of Foxe1 positive cells divided by the total number of nuclei. Ki67 staining was visually scored for the percentage of thyrocyte nuclei with positive immunostaining above the background level. At least 1,000 cells on a whole section were counted for each sample.

Immunofluorescence staining

For immunofluorescence staining of IR, and IGF-1R, thyroid tissues were cryosectioned at 8 μm thickness using a cryostat (Leica). After blocking with 10% goat serum, sections were overnight incubated with primary antibodies at 4 °C. See Supporting Information Table S1 for antibodies used. Sections were then incubated in Alexa Fluor secondary antibody. WGA (wheat germ agglutinin)-Alexa Fluor 488 conjugates was used as a membrane-staining marker. Signals were visualized with a confocal microscope (LSM 510, Carl Zeiss).

Oil Red O staining

For Oil Red O staining, 8 μm frozen thyroid sections were dried, and then washed with 60% isopropanol for 2 min. The sections were incubated with 0.1% Oil Red O solution (Sigma-Aldrich, St. Louis, MO) for 10 min at room temperature, and then rinsed with 60% isopropanol and deionized water, and counter stained with hematoxylin for 30 s.

Western blot analysis

Mouse thyroids or Nthy-ori 3–1 cells were lysed with lysis buffer (20 mM Tris–HCl, pH 7.4; 1% Triton X-100; 1 mM EDTA; 30 mM HEPES; 50 mM $Na_4P_2O_7$; 100 mM NaF) containing 1× Protease Inhibitor Cocktail (Roche Molecular Biochemicals, Indianapolis, IN) and phosphatase inhibitors. Proteins were resolved by SDS-PAGE and electrotransferred onto nitrocellulose membranes (GE Healthcare, Piscataway, NJ). See Supporting Information Table S1 for antibodies used. Immunoblotting was detected by SuperSignal West Femto Maximum Sensitivity Substrate (ThermoFisher Scientific, Fremont, CA). Densitometric quantitation was achieved using αImager 2000 (Alpha Innotech Corp., San Leandro, CA).

RNA isolation and quantitative RT-PCR analysis

Total RNA was obtained from thyroid tissues using the RNA-STAT 60 reagent (AMS Biotechnology, Abingdon, UK). To quantify transcripts, the Light Cycler System (Roche Molecular Biochemicals) was used. PCRs were performed using SYBR Green I master mix and the primers as detailed in Supporting Information Table S2. To assess the specificity of the amplified PCR products, a post-amplification melting curve analysis was performed and relative quantification was calculated using the comparative cycle threshold method.

T_3, T_4 and TSH measurements

Serum total T_3, T_4 and TSH concentrations were measured as described.[11]

IGF-1 ELISA

Serum IGF-1 levels were measured using the Quantikine Mouse/Rat IGF-I Immunoassay Kit (R&D Systems, Minneapolis, MN).

Cell culture studies

Nthy-ori 3–1, normal human differentiated thyrocytes immortalized by SV40 large-T-antigen were obtained from Sigma and maintained in 5% CO_2 at 37 °C in RPMI 1640 medium containing 10% FBS and 1% penicillin/streptomycin. After reaching confluence, the medium was changed to RPMI 1640 without FBS. For siRNA studies, cells were transiently transfected with negative control siRNA (250 nM), and IR siRNA (150 nM)/IGF-1R siRNA (100 nM) using Lipofectamine 2000 (Invitrogen, Carlsbad, CA) without penicillin and streptomycin for 4–6 h. See Supporting Information Table S3 for sequences of siRNAs used. After removing the transfection reagent, cells were incubated for 48 h in RPMI 1640 with 1% FBS medium and then stimulated with vehicle or human TSH (Sigma; 200 μU/ml) for 0–90 min. To evaluate IGF-1 effects on ErbB activation, 50 ng/ml IGF-1 (National Hormone and Peptide Program, Torrance, CA) was added to serum-starved cells for 0–75 min. For deprivation or stimulation with branched chain amino acids, cells rinsed with PBS were cultured in leucine and arginine-deficient DMEM-containing

Krebs buffer (20 mM HEPES, pH 7.4; 118 mM NaCl; 4.6 mM KCl; 1 mM MgCl$_2$, 12 mM NaHCO$_3$, 0.5 mM CaCl$_2$, 0.2% (w/v) bovine serum albumin) for 1 h and then stimulated by leucine (400 mM) and arginine (400 mM) for 10 min.[15] Cells were harvested for western blot using lysis buffer.

TUNEL assay

Apoptosis was evaluated by the TUNEL assay kit (Roche Molecular Biochemicals). TUNEL staining was performed using slides with frozen sections, incubated at 37 °C for 60 min with the TUNEL reaction mixture, which included 50 μL of enzyme solution and 450 μL of labeling solution. TUNEL-labeled cells co-localized with propidium iodide (PI) staining, were scored as apoptosis-positive nuclei.

Whole exome sequencing

Sequencing libraries for exome sequencing were constructed using SureSelect Mouse All Exome VI, and were sequenced on HiSeq 2500 (Illumina, San Diego, CA). Reads were aligned to the reference genome and somatic variants were identified as described in Materials and Methods, Supporting Information.

RNA sequencing

RNA sequencing libraries were made using the TruSeq RNA Library Kit, and sequenced on a HiSeq 2000 (Illumina). Reads were aligned into the GRCm38/mm10 mouse reference genome and analyzed as described in Materials and Methods, Supporting Information.

Statistical analysis

Data are presented as the mean ±SEM. A detailed description is available in Materials and Methods, Supporting Information.

Results

Neonatal DTIRKO mice exhibit smaller thyroids with impaired folliculogenesis

We generated DTIRKO mice by crossing IR/IGF-1R double floxed mice with Tg-Cre transgenic mice. Because Tg expression starts and folliculogenesis begins at embryonic day 15 (E15), this mouse model has utility for analyzing the role of IR and IGF-1R in thyroid folliculogenesis after completion of thyrocyte differentiation.[16] To examine potential contributions of the IR and IGF-1R in thyroid organogenesis, we euthanized mice at postnatal day 2 (P2). Body weight (BW) was not significantly different between WT and DTIRKO mice (Fig. S1*a*, Supporting Information). Expression of IR and IGF-1R was absent in the thyroid follicles of DTIRKO mice as verified by immunofluorescence and immunoblot analyses (Fig. S1*b* and *c*, Supporting Information). In DTIRKO mice at P2, thyroids were smaller than those of WT mice and folliculogenesis was defective (Fig. 1*a*). Moreover, serum T$_4$ concentrations were reduced in P14 DTIRKO mice (Fig. 1*b*), further corroborating the impairment of folliculogenesis in these mice. To determine whether impaired

folliculogenesis in DTIRKO mice was associated with thyrocyte apoptosis, TUNEL staining was performed at P2. As shown in Fig. S1*d*, Supporting Information, TUNEL positive cells were not detected in thyroids of DTIRKO or in WT mice. Furthermore, the expression of autophagy-related genes, including LC3-II, was not changed (Fig. S1*e* and *f*, Supporting Information).

The expression of Foxe1 and its target genes is reduced in neonatal DTIRKO mice

To gain insight into the molecular mechanisms by which IR/IGF-1R signaling affects thyroid folliculogenesis, we investigated the expression of *Foxe1*, a key transcription factor that plays a pivotal role in thyroid development. First, we performed western blot analysis on samples from thyroid and major non-thyroidal tissues at P5. We could not detect any FOXE1 signals in non-thyroidal organs revealing that FOXE1 is exclusively expressed in thyroids (Fig. S2*a*, Supporting Information). As illustrated in Fig. 1*c*, Foxe1-positive cells were significantly decreased in DTIRKO thyroids, whereas the expression levels of other representative TTFs, Nkx2–1 and Pax8, were not different from those in WT animals (data not shown). These results suggest that Foxe1 may be a direct downstream target of IR/IGF-1R signaling *in vivo*. In addition, transcripts of TSH-regulated genes such as *Nis, Tpo, Tg* and *Duox2* were significantly decreased in DTIRKO compared to WT thyroids (Fig. 1*d*). Collectively, these results further suggest that thyroid-specific genes regulated by the IR/IGF-1R-Foxe1 signaling cascade may play an important role in maintaining the follicular structure and the function of the postnatal thyroid.

Deletion of IR and IGF-1R paradoxically induces thyrocyte proliferation at P14

After finding impaired folliculogenesis in the thyroids of neonatal (P2) DTIRKO mice, we examined how IR and IGF-1R regulate thyroid growth later in the postnatal period. Folliculogenesis remained impaired until juvenile age (P8) (data not shown). However, there were some enlarged follicles noted at P14 in the DTIRKO thyroids (Fig. 1*e*). Of note, lipid droplets were markedly increased in DTIRKO thyroid compared to WT thyroids at P14 (Fig. S2*b*, Supporting Information). Consistent with the thyroid enlargement, the proportion of thyrocytes positive for Ki67, an indicator of cellular proliferation, was higher in P14 DTIRKO mice than in WT mice (Fig. 1*f*). To gain insight into the mechanisms involved in thyrocyte proliferation, we analyzed changes in key growth signaling pathways at P14 in the thyroid. Previous studies reported that mTOR is a critical effector of the proliferative signals initiated by TSH, through a mechanism in which Akt activation is not required.[11,17] In line with this notion, phosphorylation of mTOR, but not Akt was significantly increased in DTIRKO thyroids relative to WT thyroids (Fig. 1*g*). Ribosomal protein S6 kinase beta-1 (S6 K1),
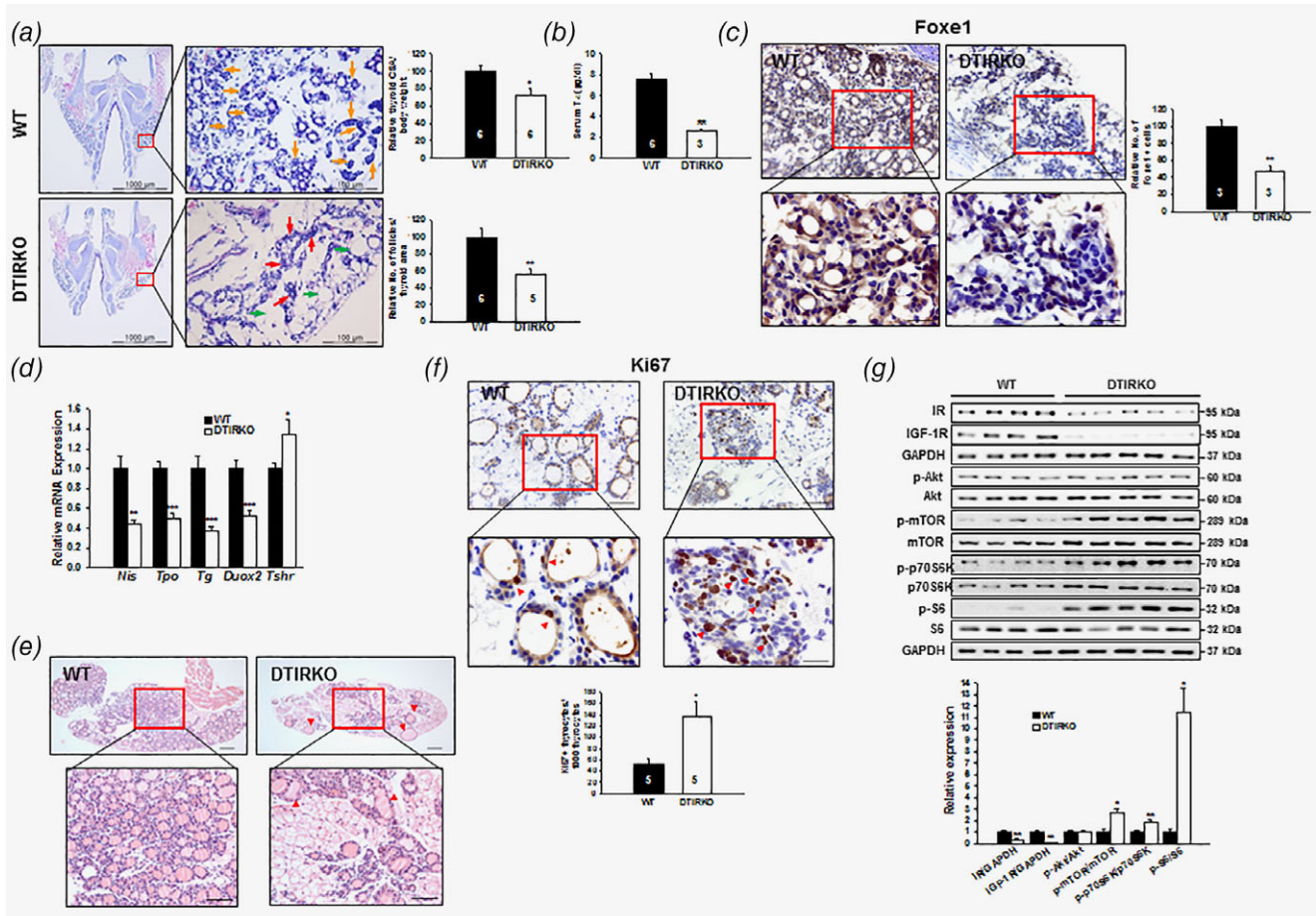
Figure 1. IR and IGF-1R are required for normal thyroid folliculogenesis. (**a**) Hematoxylin and eosin staining of coronal sections of thyroids from P2 WT and DTIRKO mice. The WT thyroid consists of well-developed round-shaped follicles with colloid-filled lumens (*orange arrows*), whereas the DTIRKO thyroid shows atrophic follicles, collapsed follicles, thyrocyte aggregates without luminal colloid (*red arrows*), and replacement of thyroid follicular tissue by fat (*green arrows*). The *right upper panel* shows relative thyroid cross sectional area (CSA) per body weight and the *right lower panel* shows relative number of spheroidal follicles per thyroid area. (**b**) Serum T_4 concentrations in P14 WT and DTIRKO mice. (**c**) Staining for Foxe1 at P2 in transverse sections from WT and DTIRKO thyroids [magnification, ×40 (×100 *insets*); scale bars, 50 μm (20 μm *insets*)]. The *right panel* shows quantification of Foxe1-positive thyrocytes. (**d**) mRNA quantification of Na^+/I^- symporter (*Nis*), thyroid peroxidase (*Tpo*), thyroglobulin (*Tg*), dual oxidase 2 (*Duox*2), and TSH receptor (*Tshr*) from the thyroids of P2 WT and DTIRKO mice. Results were normalized to β-actin and mRNA levels in WT thyroids were arbitrarily set to 1. $n = 11–13$ per group. (**e**) Hematoxylin and eosin staining of transverse sections of thyroids from P14 WT and DTIRKO mice. *Arrowheads* indicate enlarged follicles [magnification, ×10 (×20 *insets*); all scale bars, 100 μm]. (**f**) Immunohistochemical analysis of Ki67. Representative images (*upper panel*). *Arrowheads* indicate Ki67-positive proliferating thyrocytes [magnification, ×40 (×100 *insets*); scale bars, 50 μm (20 μm *insets*)]. The *lower panel* shows quantification of Ki67-positive thyrocytes per 1,000 thyrocytes. (**g**) Western blot analysis. Representative blots (*upper panel*). Densitometric ratios in thyroids from WT and DTIRKO mice (*lower panel*). Data are presented as the mean ±SEM. *, $p < 0.05$; **, $p < 0.01$; ***, $p < 0.001$ versus WT. Numbers of thyroids are indicated on the bars.

also known as p70S6 kinase (p70S6K), is a serine/threonine kinase that phosphorylates the S6 ribosomal protein (S6) to induce protein synthesis in the ribosome. We found that phosphorylation of p70S6K and its substrate S6 was markedly elevated in the thyroids of DTIRKO mice relative to WT mice (Fig. 1*g*).

TSH signaling pathways are activated during the development of follicular hyperplasia in DTIRKO thyroids
At 8 weeks of age, DTIRKO mice developed multiple large thyroid follicles (Fig. 2*a*). Some of the dilated follicles had papillary

projections and Sanderson's polsters at 24 weeks of age (Fig. 2*b*). Consistent with thyroid hyperplasia, median follicle area (Fig. 2*c*), colloid area (Fig. 2*d*) and the number of cells per follicle (Fig. 2*e*) were increased in 8-week-old DTIRKO mice relative to those in WT mice. The distribution of these parameters was greater in DTIRKO (Fig. 2*f-h*). The proportion of large follicles (> 9,000 μm²) was much higher in DTIRKO mice (36.4%) than in WT mice (2.6%) (Fig. 2*f*). Further, the proportion of follicles with colloid areas >7,000 μm² was 28-fold higher in DTIRKO mice than in WT animals (Fig. 2*g*). In contrast to WT thyroids in which the largest number of cells/follicles was
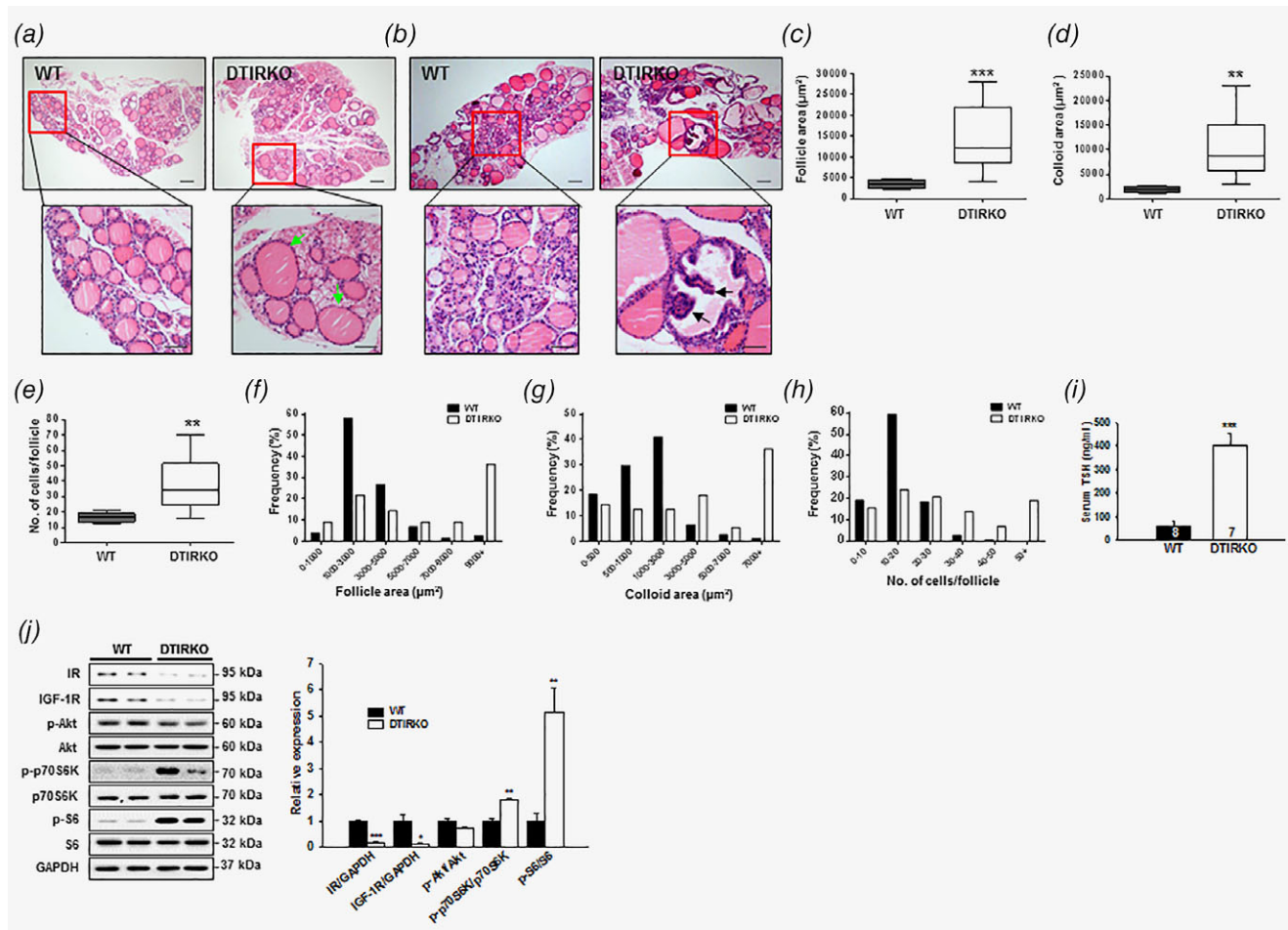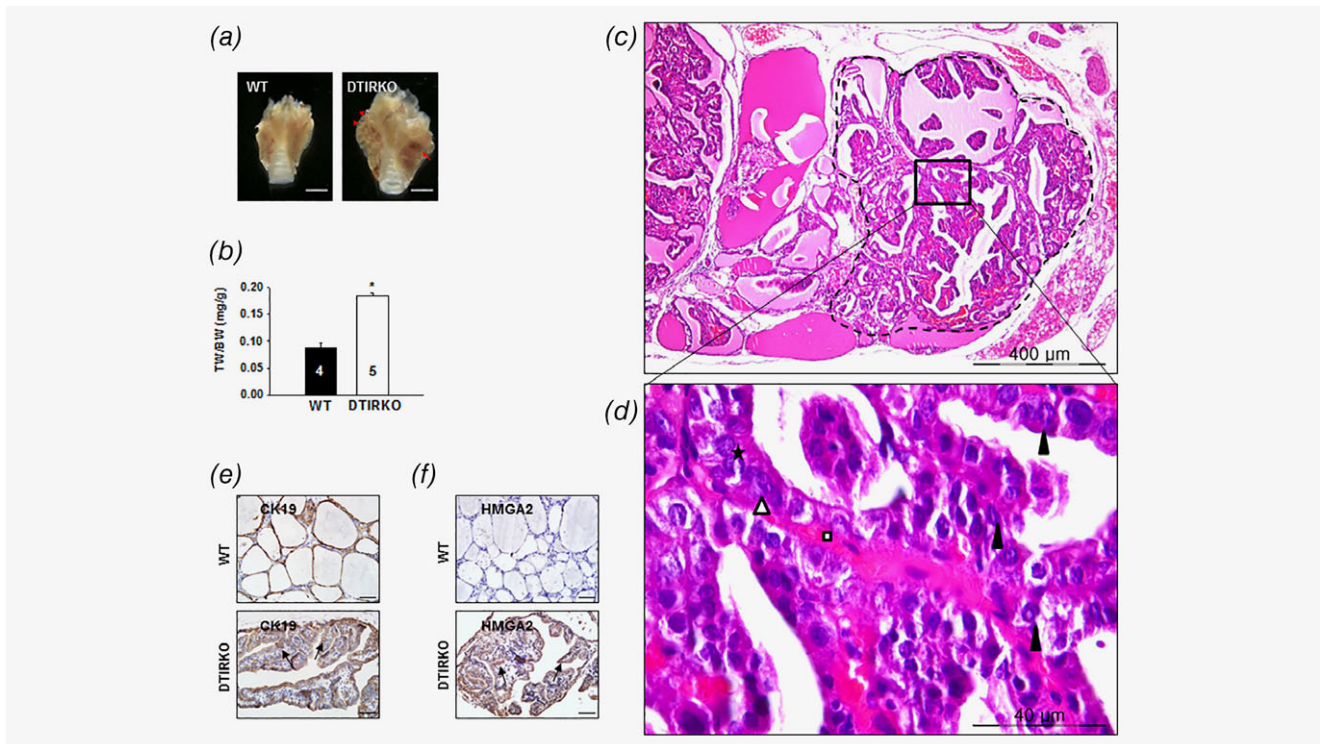
Figure 2. IR and IGF-1R deletion induces follicular hyperplasia in adult mice. (*a-b*) Hematoxylin and eosin staining of transverse sections of thyroids from 8-week-old (*a*) and 24-week-old (*b*) WT and DTIRKO mice. *Light green arrows* indicate enlarged follicles. *Black arrows* indicate papillary projections and Sanderson's polsters [magnification, ×10 (×20 insets); all scale bars, 100 µm]. (*c-h*) Morphological parameters in thyroids from 8-week-old mice were depicted using box plot (*c,d,e*) and histogram (*f,g,h*). The area of follicles (*c*) or colloids (*d*) was traced and measured in each thyroid section using Image J. The number of cells per follicle (*e*) was counted manually. The boxes represent the 25th to 75th percentiles, and horizontal lines within the box represent median values. The horizontal error bars represent the lowest and highest value in the 25th percentile minus 1.5 IQR (interquartile range) and 75th percentile plus 1.5 IQR, respectively. Three randomly selected high power fields (1 mm^2/field) per mouse were evaluated to determine the distribution of follicle area (*f*), colloid area (*g*), or number of cells per follicle (*h*). *n* = 4 per group. (*i*) Serum TSH concentrations of 8-week-old mice. (*j*) Western blot analysis. Representative blots (*left panel*). Densitometric ratios in thyroids from WT and DTIRKO mice (*right panel*). *n* = 3–4 per group. Data are presented as the mean ±SEM. *, $p < 0.05$; **, $p < 0.01$; ***, $p < 0.001$ versus WT.

10–20, the number of cells per follicle in DTIRKO mice ranged as high as >50 cells/follicle (Fig. 2*h*). Serum TSH levels were markedly enhanced in DTIRKO mice at the age of 8 weeks (Fig. 2*i*). At 24 weeks of age, serum TSH levels increased further (Fig. S3*a-c*, Supporting Information). TSH-induced thyrocyte proliferation and thyroid hyperplasia are heavily dependent on the activation of mTOR-p70S6K/S6 axis.[17] As observed in the thyroids of P14 (Fig. 1*g*), phosphorylation of p70S6K/S6 was increased in the thyroids of 8-week-old DTIRKO mice (Fig. 2*j*). Collectively, these results suggest that sustained TSH overproduction contributes to the development and progression of thyroid hyperplasia in DTIRKO mice, at least in part, through activation of p70S6K/S6 signaling.

Aged DTIRKO mice spontaneously developed papillary thyroid carcinoma (PTC)-like lesions

In a 50-week follow-up, DTIRKO thyroids exhibited a grossly enlarged and lobulated morphology and contained small tumors (Fig. 3*a*). The thyroid weight to body weight (TW/BW) ratio, was markedly increased in DTIRKO relative to WT mice (Fig. 3*b*). Microscopically, all DTIRKO mice examined developed PTC-like lesions[18] which showed characteristic nuclear abnormalities, such as nuclear enlargement and overlapping, membrane irregularity, chromatin clearing and occasional nuclear grooves (Fig. 3*c*, 3*d* and Table S4, Supporting Information). In contrast, in a 50-week follow-up, TIGF1RKO thyroids exhibited focal areas of follicular hyperplasia, but the typical nuclear features of PTC were not seen

Figure 3. IR and IGF-1R deletion spontaneously induces papillary thyroid carcinoma (PTC)-like lesions with aging. (*a*) Representative images of thyroid from 50-week-old WT and DTIRKO mice. *Arrowheads* indicate hyperplastic follicles and *arrow* indicates small tumor. (*b*) TW/BW ratio in 50-week-old WT and DTIRKO mice. (*c,d*) Hyperplastic and PTC-like lesions in 50-week-old DTIRKO mice. (*c*) Hematoxylin and eosin stain of DTIRKO mouse thyroid gland. PTC-like areas are marked with a dotted line [magnification, ×100]. (*d*) Higher magnification of the PTC-like lesion. Cells show characteristic nuclear features of PTC - nuclear enlargement (*star*) and overlapping (*triangle*), membrane irregularity, chromatin clearing (*rectangle*), and occasional nuclear grooves (*arrowheads*) [magnification, ×1,000]. Immunohistochemical staining for CK19 (*e*), and HMGA2 (*f*) of thyroid sections from WT and DTIRKO mice. *Arrows* indicate positive staining. Magnification, ×40; scale bars, 50 μm. Data are presented as the mean ±SEM. *, $p < 0.05$ versus WT. Numbers of thyroids are indicated on the bars.

(Fig. S4, Supporting Information). The PTC-like lesions formed in DTIRKO mice did not show vascular invasion or thyroid capsule or extrathyroidal extension (data not shown). Cytokeratin (CK)-19 and anti-high mobility group AT-hook 2 (HMGA2) are immunomarkers for distinguishing PTC-like lesions from other follicular lesions.[19] Thus, we performed immunohistochemical staining for these markers and found that both were highly expressed in DTIRKO thyroids, but were largely absent in WT thyroids (Fig. 3*e*, 3*f*). To investigate potential genomic alterations that initiate formation of PTC-like lesions, whole-exome sequencing with one tumor mass and one skeletal muscle (control) from the same 50-week-old DTIRKO mouse was performed. The rearrangement of the *RET* gene in PTC (RET/PTC) or point mutations of the BRAF and RAS genes, which are most commonly detected in human PTC patients,[20] were not found in DTIRKO thyroid. Moreover, changes in some other cancer-associated genomic mutations were not detected (Table S5, Supporting Information).

Development of PTC-like lesions may be the consequence of aberrant EGFR signaling

We conducted RNA sequencing (RNA-seq) analyses in thyroids from 50-week-old WT and DTIRKO mice to investigate

potential genes that could contribute to the PTC phenotype. The pathway analysis tool iPathwayGuide identified potential biological pathways (Fig. S5*a*, Supporting Information). ErbB signaling is known to be associated with PTC.[21] The ErbB family of receptor tyrosine kinases includes epidermal growth factor receptor (EGFR; also known as ErbB1), ErbB2, ErbB3 and ErbB4. mRNA expression of ErbB2 and ErbB3 are highly induced in PTC specimens, and EGFR has been implicated in proliferation, migration and invasion of thyroid cancer cells *in vitro* and *in vivo*.[22,23] DTIRKO thyroids significantly induced expression of genes involved in EGFR signaling (Fig. S5*b*, Supporting Information). We verified the induction of EGFR, ErbB2 and ErbB3 by quantitative RT-PCR (Fig. S6, Supporting Information). Furthermore, EGFR-, p-EGFR-, ErbB2- and ErbB3-positive immunostaining was detectable to a much greater extent in the thyroids of DTIRKO than in WT mice (Fig. 4*a-d*). Consistently, western blot analysis showed elevated expression and phosphorylation of EGFR and ErbB2, and the downstream phosphorylation of Erk were also increased in DTIRKO thyroids (Fig. 4*e*). However, EGFR ligands such as EGF, heparin-binding EGF-like growth factor (HB-EGF) and transforming growth factor-alpha (TGF-α)
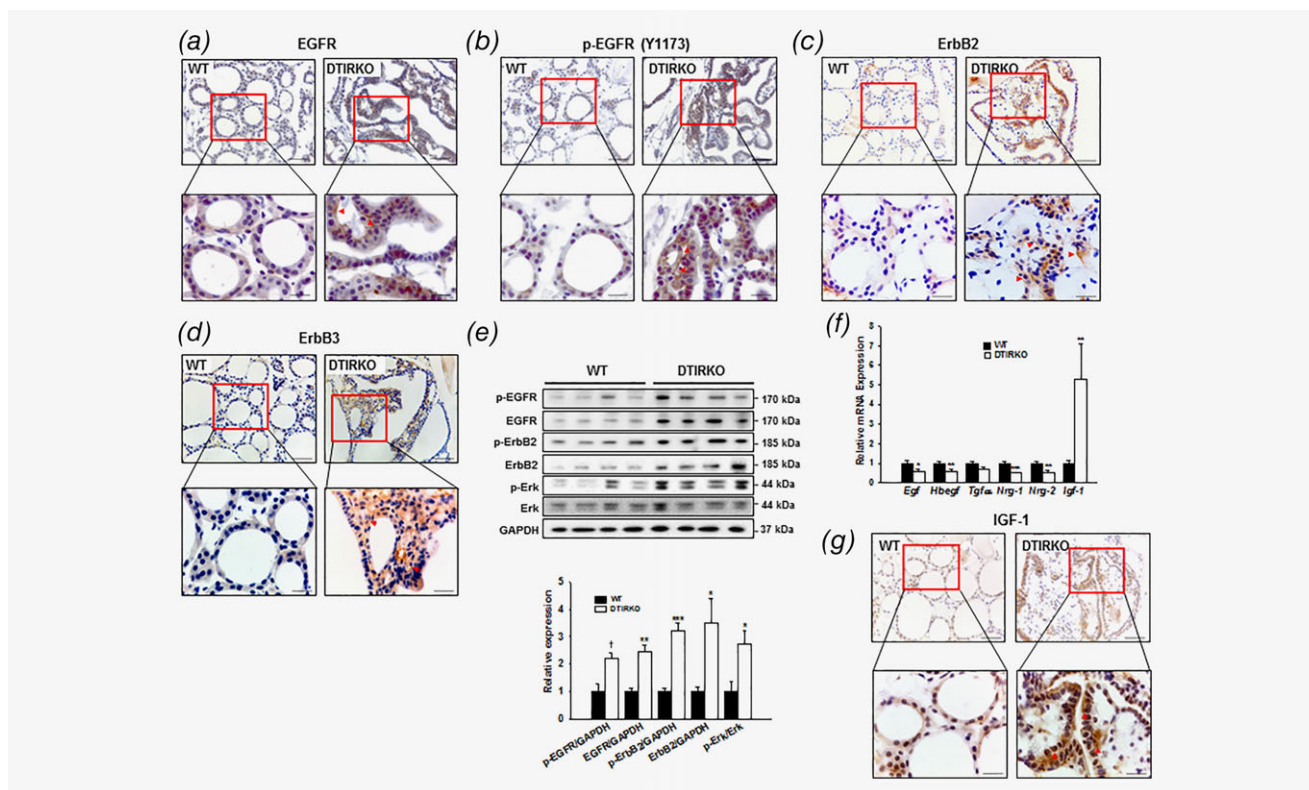
Figure 4. Aged DTIRKO mice show induction of ErbB family proteins and IGF-1 in thyroid. Representative immunohistochemical staining for EGFR (*a*), p-EGFR (*b*), ErbB2 (*c*), and ErbB3 (*d*) in thyroid sections from 50-week-old WT and DTIRKO mice. *Arrowheads* indicate positive membrane staining [magnification, ×40 (×100 *insets*); scale bars, 50 μm (20 μm *insets*)]. (*e*) Western blot analysis (*upper panel*) and densitometric ratios (*lower panel*) of p-EGFR, EGFR, p-ErbB2, ErbB2, and Erk phosphorylation in thyroids from WT and DTIRKO mice. *n* = 4 per group. (*f*) mRNA quantification of EGF, heparin-binding EGF-like growth factor (HB-EGF), transforming growth factor-alpha (TGF-α), neuregulin (Nrg)-1, Nrg-2, and IGF-1. Results were normalized to β-actin mRNA levels in WT thyroids and arbitrarily set to 1. *n* = 8–11 per group. (*g*) Representative immunohistochemical staining for IGF-1. *Arrowheads* indicate positive staining. Magnification, ×40 (×100 *insets*); scale bars, 50 μm (20 μm *insets*). Data are presented as the mean ±SEM. †, *p* = 0.057; *, *p* < 0.05; **, *p* < 0.01; ***, *p* < 0.001 versus WT.

and ErbB3 ligands neuregulin (Nrg)-1 and Nrg-2 were not induced in DTIRKO thyroids (Fig. 4*f*). In contrast to mice bearing PTC-like lesions at 50 weeks of age, there was no pronounced expression of EGFR, p-EGFR, ErbB2 and ErbB3 in 8-week-old DTIRKO thyroids (Fig. S7, Supporting Information). Although no difference was found in serum IGF-1 levels in WT versus DTIRKO mice of three age groups (Fig. S8, Supporting Information), local expression of thyroid IGF-1 transcript (Fig. 4*f*) and protein (Fig. 4*g*) was increased in 50-week-old DTIRKO mice, suggesting induction of IGF-1 may be involved in autocrine transactivation of some ErbB family members.

To further evaluate the contribution of increased TSH and IGF-1 levels to ErbB signaling and to obtain direct evidence that the IR/IGF-1R axis is a negative regulator of the ErbB signaling in thyrocytes, we utilized Nthy-ori 3–1 cells transfected with control siRNA or subjected to simultaneous knockdown of IR and IGF-1R with IR/IGF-1R siRNA. IR/IGF-1R silencing significantly increased both EGFR protein expression and EGFR phosphorylation, but not ErbB2 and ErbB3 phosphorylation and expression (Fig. 5). Notably, TSH further

stimulated EGFR phosphorylation in IR/IGF-1R knockdown cells. We then determined whether IGF-1 might transactivate EGFR. IGF-1 stimulation enhanced both phosphorylation and expression of EGFR in IGF-1 treated IR/IGF-1R knockdown cells (Fig. 6). These data suggest that autocrine/intracrine IGF-1 in concert with TSH could aberrantly activate the overexpressed EGFR in thyrocytes of DTIRKO mice. Together, these findings indicate that overproduction of TSH and IGF-1 as a consequence of simultaneous knockout of IR/IGF-1R signaling in DTIRKO mice induces PTC-like lesions through aberrant activation of EGFR signaling.

Discussion

We previously showed that single deletion of either IR or IGF-1R alone in the thyroid does not cause postnatal thyroid dysgenesis.[10,11] In our study, we demonstrate that normal folliculogenesis is dependent upon the presence of both IR and IGF-1R in the thyroid. TTFs such as Nkx2–1, Foxe1 and Pax8, are expressed in follicular progenitor cells at E8.5 in mice. After sequential developmental stages of expansion of the thyroid primordium (E9.5), migration (E11.5) and
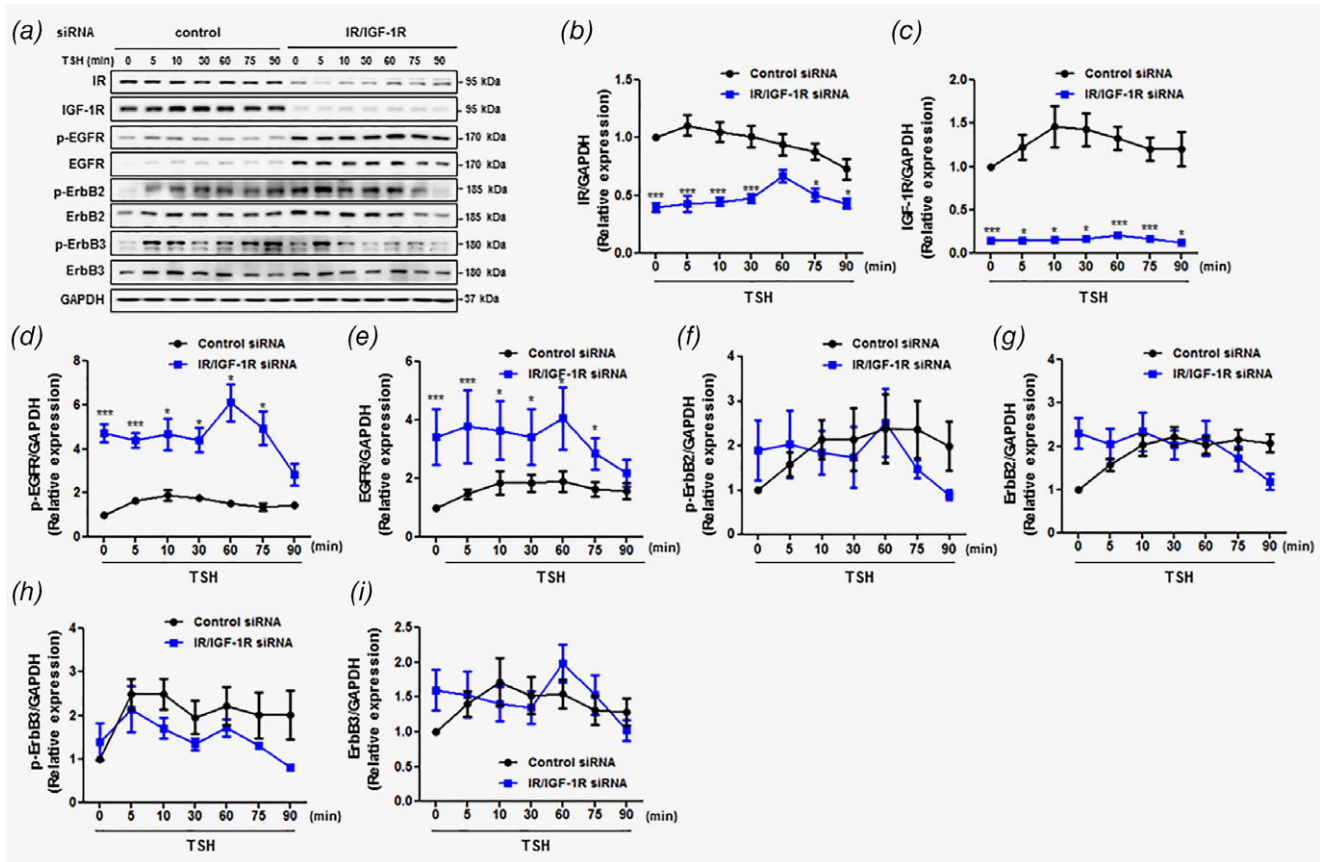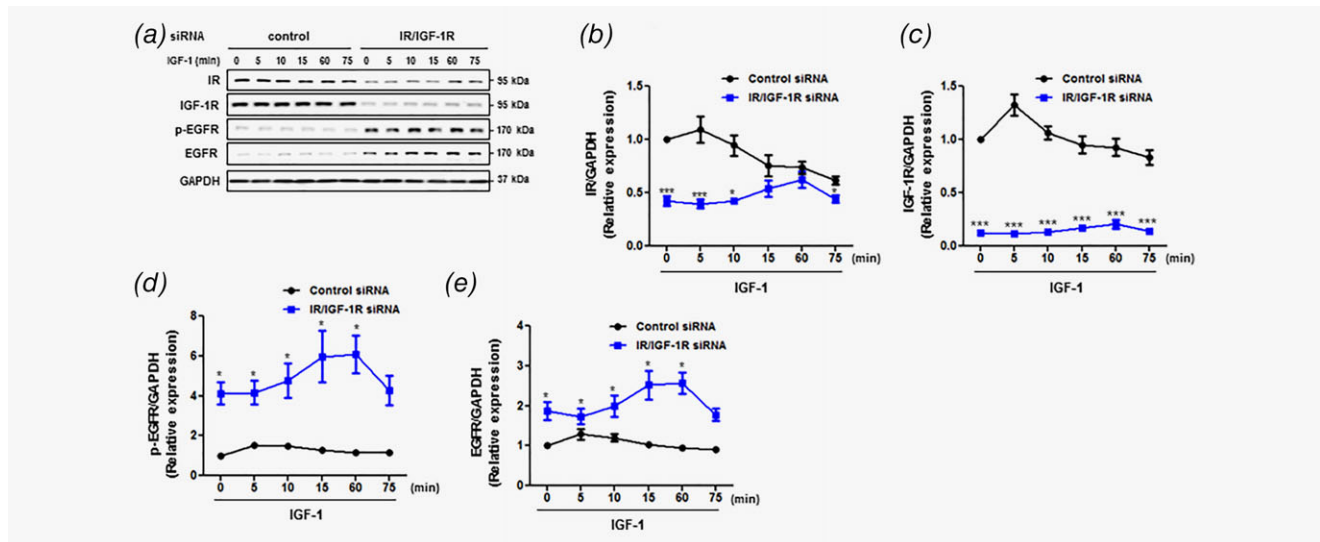
Figure 5. IR/IGF1R depletion and/or TSH stimulation activate ErbB signaling in the human thyroid cell line Nthy-ori 3–1. Cells were pretreated with control siRNA or IR/IGF-1R siRNA for 48 h and then incubated with 200 μU/ml of bovine TSH for 0–90 min. Western blot analysis (**a**) and densitometric ratios (**b-i**) of IR, IGF-1R, p-EGFR, EGFR, p-ErbB2, ErbB2, p-ErbB3, and ErbB3. There were overall between group differences with respect to IR, IGF-1R, p-EGFR, EGFR, ErbB2 and p-ErbB3 ($F_{(7,4)}$ = 19.733; p = 0.006; Wilks' λ = 0.028; partial η^2 = 0.97, $F_{(7,4)}$ = 70.524; p = 0.001; Wilks' λ = 0.756; partial η^2 = 0.992, $F_{(7,4)}$ = 16.791; p = 0.008; Wilks' λ = 0.033; partial η^2 = 0.967, $F_{(7,4)}$ = 7.775; p = 0.033; Wilks' λ = 0.068; partial η^2 = 0.932, $F_{(6,3)}$ = 10.306; p = 0.041; Wilks' λ = 0.046; partial η^2 = 0.954, and $F_{(7,4)}$ = 8.352; p = 0.029; Wilks' λ = 0.064; partial η^2 = 0.936, respectively). However, there was no evidence of statistically significant differences between groups with respect to p-ErbB2 and ErbB3 ($F_{(7,4)}$ = 0.910, p = 0.615: Wilks' λ = 0.239: partial η^2 = 0.761 and ($F_{(7,4)}$ = 3.070; p = 0.148; Wilks' λ = 0.157; partial η^2 = 0.843). Comparisons with control siRNA at each time points are presented as *, $p < 0.05$; **, $p < 0.01$ and ***, $p < 0.001$.

proliferation of precursor cells (E14.5), thyroid folliculogenesis begins at E15. At E16.5, thyroid differentiation and organogenesis are completed. In addition, TSH target genes, *Tg, Tpo* and *Tshr* are expressed at E14.5 and *Nis* and *Duox2* at E15.5 [2]. T_4 is detected at E16.5.[1,5] Thus, the coordinated expression of TTFs is essential not only for thyroid folliculogenesis, but also for the functional differentiation of the thyroid.[2,5] However, until now, upstream regulators of TTFs that control folliculogenesis during the late stage of thyroid organogenesis were incompletely understood. It has been proposed that TSH, insulin, or IGF-1 increases the levels of Foxe1 in a rat thyroid cell line.[24] Although TSH signaling is required for the expression of *Nis* and *Tpo* genes before birth, thyroid organogenesis is TSH-independent because thyroids of TSHR KO or mice that lack TSH exhibit normal postnatal thyroid size, that decreases in size 2 months after birth.[3,4,25] Consequently, embryonic TSH does not play an equivalent role in controlling thyroid growth in the adult.[3] It is noteworthy that insulin modulates *Tg* and *Tpo* gene transcription by regulating the levels of Foxe1 DNA binding activity through the IGF-1 receptor.[21] Furthermore, insulin/IGF-1 induces Foxe1 protein expression in the rat thyroid cell line FRTL-5.[9] Foxe1 recognizes and binds to a consensus DNA sequence present in *Tg*,[9] *Tpo*,[26] *Nis*, [27] and *Duox2*.[27] DTIRKO thyroids show a decrease in the expression of these genes and these changes likely account for follicular dysgenesis of DTIRKO thyroids. As endogenous Tg expression starts at E15 and Cre-mediated recombination is therefore likely to begin before birth,[13,16] Tg-Cre mediated inactivation of IR/IGF-1R is a suitable model for studying their roles in folliculogenesis, which normally occurs from E15 to E21 in the mouse. However, it should be pointed out that IR/IGF-1R does not seem to regulate other transcription factors such as Nkx2–1, and Pax8, so that neonatal DTIRKO follicles could contain heterogeneous

Figure 6. IR/IGF-1R depletion and/or IGF-1 stimulation activate ErbB signaling in the human thyroid cell line Nthy-ori 3−1. Cells were pretreated with control siRNA or IR/IGF-1R siRNA for 48 h and then incubated with 50 ng/ml IGF-1 for 0−75 min. Western blot analysis (***a***) and densitometric ratios (***b-e***) of IR, IGF-1R, p-EGFR, and EGFR. There were overall between group differences with respect to IR, IGF-1R, p-EGFR and EGFR (F (6,5) = 26.478; p = 0.001; Wilks' λ = 0.031; partial η^2 = 0.969, F (6,5) = 235.541; $p < 0.001$; Wilks' λ = 0.004; partial η^2 = 0.996, F (6,5) = 19.116; p = 0.003; Wilks' λ = 0.042; partial η^2 = 0.958, and F (1,18.483) = 19.631; p = 0.001; partial η^2 = 0.663, respectively). Comparisons with control siRNA at each time points are presented as *, $p < 0.05$; **, $p < 0.01$ and ***, $p < 0.001$.

populations of cells with varying degrees of differentiation. Thus, further studies to identify the mechanism by which IR/IGF-1R signaling regulates thyroid precursor cells are warranted.

Increased circulating TSH likely causes thyroid hyperplasia and compensates for the loss of IGF-1R signaling without increasing adult thyroid weight in thyrocyte-selective IGF-1R KO mice.[12] We also maintained independent IGF-1R KO mouse colonies in our facility and found similar phenotypes after 16 weeks of age (unpublished data). Thus, the DTIRKO thyroid could be similarly stimulated by increased TSH. To address this issue, we analyzed DTIRKO mice from P3 to P14. However, we did not observe any evidence of increased thyrocyte proliferation in DTIRKO mice before P14, indicating that a longer period of TSH stimulation might be necessary to initiate thyrocyte proliferation in these mice. Whether undifferentiated thyrocytes are more susceptible to proliferate in response to TSH stimulation remains unknown. We could not confirm that primary hypothyroidism also developed in P14 DTIRKO mice because the amount of serum to measure TSH at this age of mice was insufficient. Despite this limitation, we posit that, not only low T_4 levels but also reduced numbers of follicles in DTIRKO mice may contribute to primary hypothyroidism at this early stage.

The mTOR/S6K axis plays a key role in controlling the thyroid proliferative response to chronic TSHR stimulation through Akt-independent mechanisms *in vitro* and *in vivo*.[17,28] It is plausible that increased availability of amino acids enhances mTOR/p70S6K signaling in the insulin resistance state. Theoretically, defective IR/IGF-1R signaling in thyrocytes could give rise to changes in nutrient availability such as

decreased glucose utilization and increased amino acid availability, leading to the direct activation of mTOR.[15,29] Under normal growth conditions, IR/IGF-1R knockdown in a human thyroid cell line, Nthy-ori 3−1 revealed no differences in mTOR/p70S6K/S6 phosphorylation relative to controls (Fig. S9, Supporting Information). As expected, addition of amino acids, after withdrawal of amino acids for 1 h, induced the mTOR signaling pathway. However, we determined that adding back an amino acid mixture to the medium did not induce a further increase in mTOR/p70S6K/S6 phosphorylation in IR/IGF-1R double-knockdown cells. This suggests that the amino acid sensitivity might not be a primary cause for the mTOR activation observed *in vivo*. Thus, it is possible that the compensatory increase of TSH contributed to the initiation of thyrocyte proliferation in DTIRKO mice. In addition, our genetically engineered mouse model argues against the traditional view that TSH in cooperation with insulin or IGF-1 stimulates cell cycle progression and proliferation in the thyroid.[8]

In our study, we demonstrated an oncogenic role for the ErbB signaling pathway in enhancing TSH-induced follicular hyperplasia. Thyroid carcinoma is the most common endocrine malignancy. PTCs are follicular thyroid cell-derived tumors accounting for the majority of thyroid cancer.[30] Although there is an association between higher serum concentrations of TSH and a higher risk for malignancy of thyroid nodules in mouse[31] and humans,[32] TSH does not seem to initiate thyroid carcinoma. For example, somatic mutations in the TSHR are observed in benign functioning thyroid adenomas with low risk of malignant transformation.[33,34] In contrast, the MAPK pathway is primarily involved in PTC. Indeed, BRAF[V600E] point mutations are detected in more

Cancer Genetics and Epigenetics

than half of early stage PTC patients, which results in the activation of the Mek–Erk cascade, that drives the development of PTC.[30] A mouse model with a knock-in of oncogenic BRAF[V600E] gave rise to invasive PTC and concomitantly became hypothyroid as demonstrated by high TSH levels. When BRAF[V600E] knock-in mice were crossed with TSHR knockout mice, the double mutant mice developed low-grade, smaller and less invasive PTC indicating TSH *per se* may not be oncogenic, but increased TSH levels are likely to contribute to PTC progression.[4] Our results show that acquisition of BRAF[V600E] or other genomic mutations might not be the exclusive mediators leading to the development of PTC-like lesions. We analyzed potential genomic alterations based on whole-exome sequencing and found no evidence of other oncogenic mutations. However, because only one animal was used for each experimental group, we cannot exclude the possibility of genetic variation in these loci across different animals.

Our findings highlight EGFR, ErbB2 and ErbB3 as potential candidates, which we believe could be pro-oncogenic, as cancer cells typically express multiple receptor tyrosine kinases.[35] Although EGFR mutations have been reported in a minority of patients with PTC,[36] the EGFR protein was significantly induced in thyroid carcinoma, especially in poorly differentiated carcinoma suggesting a role in its progression and aggressiveness.[37] The reciprocal relationship between IR/IGF-1R and ErbB signaling appears to be an important pathophysiologic mechanism for PTC-like lesions in our model. Knockdown of IR/IGF-1R in cultured human thyrocytes *per se* is sufficient to increase ErbB signaling resulting from induction of EGFR protein and autophosphorylation. In addition, TSH transactivates EGFR in the absence of IR/IGF-1R, together pointing to aberrant ErbB signaling from IR/IGF-1R deletion-associated EGFR autophosphorylation. It is possible that TSH overproduction during thyroid hyperplasia in DTIRKO mice, in turn, activates EGFR signaling, which contributes to PTC formation. This hypothesis is supported by Buch *et al.* showing that EGFR transactivation by TSH was additionally involved in MAPK signaling in thyroid follicular carcinoma cell line but not in nonneoplastic primary thyrocytes.[38] To definitively prove a positive feedback loop between the TSH and the EGFR axis, TSH gene silencing or EGFR signaling blockade studies are needed in future. Although ErbB2 and ErbB3 are highly expressed in PTC specimens,[21] whether induction of ErbB is a primary or secondary oncogenic event

in a subgroup of PTC patients without genomic alterations is not clear at this point. Based on our preliminary immunohistochemical analysis, EGFR was strongly stained in PTC patients (data not shown). Future human studies will be required to clarify the interaction between IR/IGF-1R and ErbB in tumor cells.

Although our data do not identify the specific ligands for ErbB family proteins, it is interesting to note that local production of IGF-1 is induced in DTIRKO thyroid. IGF-1 stained only PTC areas in DTIRKO thyroids. Therefore, tumor-cell derived autocrine IGF-1 could promiscuously activate the EGFR to contribute to activation of the Erk/c-Myc oncogenic pathway. We speculate that loss of IR/IGF-1R drives a compensatory overproduction of local IGF-1 in an autocrine loop. Thus, anti-cancer therapies involving the inhibition of the IR or IGF-1R signaling could potentially have the undesired off-target adverse effects by inducing compensatory proliferation signals such as oncogenic IGF-1.

In our study, DTIRKO mice displayed cellular atypia and increased expression of CK19 and HMGA2, which are characteristics of PTC. While the progressive nature of PTC-like lesions is typified by local invasion or distant metastasis, we were unable to find evidence for vascular invasion, extrathyroidal extension, or lymph node metastasis in 50-week-old DTIRKO mice, which is the basis for using the term PTC-like lesion instead of PTC. However, we would like to highlight that the loss of IR/IGF-1R in thyrocytes in concert with elevated TSH levels and aberrant EGFR activation could initiate carcinogenesis without any genomic mutations.

In conclusion, we provide genetic evidence that the availability of both IR and IGF-1R is a prerequisite for neonatal thyroid folliculogenesis. Furthermore, our study provides novel insights into how crosstalk between IR/IGF-1R and TSH or ErbB signaling systems may underlie thyroid carcinogenesis.

References

1. De Felice M, Di Lauro R. Thyroid development and its disorders: genetics and molecular mechanisms. *Endocr Rev* 2004;25:722–46.
2. Braverman LE, Cooper DS, eds. *Werner and Ingbar's The Thyroid*, 10th ed. Philadelphia: Lippincott Williams & Wilkins 2012;4–23.
3. Postiglione M, Parlato R, Rodriguez-Mallon A, et al. Role of the thyroid-stimulating hormone receptor signaling in development and differentiation of the thyroid gland. *Proc Natl Acad Sci* 2002;99:15462–7.
4. Franco AT, Malaguarnera R, Refetoff S, et al. Thyrotrophin receptor signaling dependence of Braf-induced thyroid tumor initiation in mice. *Proc Natl Acad Sci* 2011;108:1615–20.
5. Fernández LP, López-Márquez A, Santisteban P. Thyroid transcription factors in development, differentiation and disease. *Nat Rev Endocr* 2015;11:29–42.
6. Nakae J, Kido Y, Accili D. Distinct and overlapping functions of insulin and IGF-I receptors. *Endocr Rev* 2001;22:818–35.
7. S-I T, Conti M, Van Wyk JJ. Thyrotropin potentiation of insulin-like growth factor-I dependent deoxribonucleic acid synthesis in FRTL-5 cells: mediation by an autocrine amplification factor (s). *Endocrinology* 1990;126:736–45.
8. Kimura T, Van Keymeulen A, Golstein J, et al. Regulation of thyroid cell proliferation by TSH and other factors: a critical evaluation of in vitro models. *Endocr Rev* 2001;22:631–56.
9. Santisteban P, Acebron A, Polycarpou-Schwarz M, et al. Insulin and insulin-like growth

factor I regulate a thyroid-specific nuclear protein that binds to the thyroglobulin promoter. *Mol Endocrinol* 1992;6:1310–7.

10. Ock S, Lee SH, Ahn J, et al. Conditional deletion of insulin receptor in thyrocytes does not affect thyroid structure and function. *Endocr J* 2011;58: 1013–9.

11. Ock S, Ahn J, Lee SH, et al. IGF-1 receptor deficiency in thyrocytes impairs thyroid hormone secretion and completely inhibits TSH-stimulated goiter. *FASEB J* 2013;27:4899–908.

12. Müller K, Führer D, Mittag J, et al. TSH compensates thyroid-specific IGF-I receptor knockout and causes papillary thyroid hyperplasia. *Mol Endocrinol* 2011;25:1867–79.

13. Kero J, Ahmed K, Wettschureck N, et al. Thyrocyte-specific G q/G 11 deficiency impairs thyroid function and prevents goiter development. *J Clin Investig* 2007;117:2399–407.

14. Bychkov A, Saenko V, Nakashima M, et al. Patterns of FOXE1 expression in papillary thyroid carcinoma by immunohistochemistry. *Thyroid* 2013;23:817–28.

15. Kim S, Kim SF, Maag D, et al. Amino acid signaling to mTOR mediated by inositol polyphosphate multikinase. *Cell Metab* 2011;13:215–21.

16. Undeutsch H, Löf C, Offermanns S, et al. A mouse model with tamoxifen-inducible thyrocyte-specific cre recombinase activity. *Genesis* 2014;52:333–40.

17. Brewer C, Yeager N, Di Cristofano A. Thyroid-stimulating hormone–initiated proliferative signals converge in vivo on the mTOR kinase without activating AKT. *Cancer Res* 2007;67:8002–6.

18. Patyra K, Jaeschke H, Löf C, et al. Partial thyrocyte-specific Gαs deficiency leads to rapid-onset hypothyroidism, hyperplasia, and papillary thyroid carcinoma–like lesions in mice. *FASEB J* 2018;32.

19. Charles R-P, Iezza G, Amendola E, et al. Mutationally activated BRAFV600E elicits papillary thyroid cancer in the adult mouse. *Cancer Res* 2011;71:3863–71.

20. Kondo T, Ezzat S, Asa SL. Pathogenetic mechanisms in thyroid follicular-cell neoplasia. *Nat Rev Cancer* 2006;6:292–306.

21. Haugen D, Akslen L, Varhaug J, et al. Expression of c-erbB-2 protein in papillary thyroid carcinomas. *Br J Cancer* 1992;65:832–7.

22. Kato S, Kobayashi T, Yamada K, et al. Expression of erbB receptors mRNA in thyroid tissues. *Biochim Biophys Acta-General Subjects* 2004;1673: 194–200.

23. Hoelting T, Siperstein AE, Clark OH, et al. Epidermal growth factor enhances proliferation, migration, and invasion of follicular and papillary thyroid cancer in vitro and in vivo. *J Clin Endocrinol Metab* 1994;79:401–8.

24. Ortiz L, Zannini M, Di Lauro R, et al. Transcriptional control of the forkhead thyroid transcription factor TTF-2 by thyrotropin, insulin, and insulin-like growth factor I. *J Biol Chem* 1997;272:23334–9.

25. Marians R, Ng L, Blair H, et al. Defining thyrotropin-dependent and -independent steps of thyroid hormone synthesis by using thyrotropin receptor-null mice. *Proc Natl Acad Sci* 2002;99: 15776–81.

26. Aza-Blanc P, Di Lauro R, Santisteban P. Identification of a cis-regulatory element and a thyroid-specific nuclear factor mediating the hormonal regulation of rat thyroid peroxidase promoter activity. *Mol Endocrinol* 1993;7:1297–306.

27. Fernández LP, López-Márquez A, Martínez ÁM, et al. New insights into FoxE1 functions: identification of direct FoxE1 targets in thyroid cells. *PLoS One* 2013;8:e62849.

28. Suh JM, Song JH, Kim DW, et al. Regulation of the phosphatidylinositol 3-kinase, Akt/protein kinase B, FRAP/mammalian target of rapamycin, and ribosomal S6 kinase 1 signaling pathways by thyroid-stimulating hormone (TSH) and stimulating type TSH receptor antibodies in the thyroid gland. *J Biol Chem* 2003;278:21960–71.

29. Malmberg SE, Adams CM. Insulin Signaling and the General Amino Acid Control Response Two distinct pathways to amino acid synthesis and uptake. *J Biol Chem* 2008;283:19229–34.

30. Xing M. Molecular pathogenesis and mechanisms of thyroid cancer. *Nat Rev Cancer* 2013;13: 184–99.

31. Schaller RT Jr, Stevenson JK. Development of carcinoma of the thyroid in iodine-deficient mice. *Cancer* 1966;19:1063–80.

32. Boelaert K, Horacek J, Holder R, et al. Serum thyrotropin concentration as a novel predictor of malignancy in thyroid nodules investigated by fine-needle aspiration. *J Clin Endocr Metab* 2006; 91:4295–301.

33. Parma J, Duprez L, Van Sande J, et al. Somatic mutations in the thyrotropin receptor gene cause hyperfunctioning thyroid adenomas. *Nat* 1993; 365:649–51.

34. Bourasseau I, Savagner F, Rodien P, et al. No evidence of thyrotropin receptor and GSα gene mutation in high iodine uptake thyroid carcinoma. *Thyroid* 2000;10:761–5.

35. Wilson TR, Fridlyand J, Yan Y, et al. Widespread potential for growth-factor-driven resistance to anti-cancer kinase inhibitors. *Nature* 2012;487:505–9.

36. Murugan AK, Dong J, Xie J, et al. Uncommon GNAQ. MMP8, AKT3, EGFR, and PIK3R1 mutations in thyroid cancers. *EndocrPathol* 2011;22: 97–102.

37. Landriscina M, Pannone G, Piscazzi A, et al. Epidermal growth factor receptor 1 expression is upregulated in undifferentiated thyroid carcinomas in humans. *Thyroid* 2011;21:1227–34.

38. Büch TR, Biebermann H, Kalwa H, et al. G13-dependent activation of MAPK by thyrotropin. *J Biol Chem* 2008;283:20330–41.

Cancer Genetics and Epigenetics